Ab initio Calculation for Photocurrent in Silicon p-n Junction: the First-Order Perturbation Theory

Majid Ghandchi *, Hossein Fazlalipour
Department of Electrical Engineering. Ahar Branch, Islamic Azad University, Ahar, Iran
Email: majid.ghandchi@gmail.com, h-fazlalipour@iua-ahar.ac.ir

Abstract

A computational study based on first-principles calculations by supercomputers for nanoelectronic devices sometimes leads to results that can rarely be obtained in experimental laboratories with measuring tolerances. In this paper, therefore, we obtained the electronic, electrical, and optoelectrical properties of silicon p-n junction nanostructures by solving Non-Equilibrium Green's Function (NEGF) using the first-order perturbation theory. We extracted the density of states (DOS), quantum carrier transport coefficient, IV-curve, and optoelectrical behavior by calculating the photocurrent and then plotted the light absorption spectrum. In the studied silicon nanostructure, light absorption is negligible for incident photon energy below 1 eV, and peak absorption occurs at 4 eV. In this research, the developed computational model paves the way for the study of nano-opto-electronic devices.

Keywords: Photocurrent, *Non-equilibrium Green's function (NEGF), density functional theory (DFT), IV characteristics*.

1. Introduction

The conversion of optical energy into electrical energy is important from two aspects. First, solar cells and the use of sunlight energy to generate electricity is a very attractive field for researchers and industries related to solar cells [1]. The second aspect concerns the use of photodetectors not only in fiber optic communication [2] but also for imaging in various fields, including medical engineering [3]. All these cases indicate that appropriate models with sufficient accuracy to extract the optical behavior of nano-devices by involving all quantum effects without applying common approximations to the bulk condition should be developed to study the optical behavior of nanostructures.

The photocurrent is produced by various mechanisms. After photon energy absorption in a structure, an electrical signal is generated from this absorbed energy in different means. With an emphasis on silicon and other semiconductor materials, we introduce five common physical mechanisms in the following: *(i)* In the photovoltaic effect [4], we observe the generation of photocurrent resulting from the separation of electron-hole pairs by the built-in electric field in the p-n metallurgical junction. *(ii)* In photothermoelectric (PTE), the generation of hot electrons produces a V_{PTE} voltage based on the Seebeck effect [5]. *(iii)* The bolometer method refers to changing the electrical conductance and carrier transport properties of an illuminated material due to absorption heat [6] This type of photodetection considers the thermal resistance of R_h and ΔR creation by ΔT. *(iv)* The photogating method [7] with light illumination results in the creation of Δn, and the photogenerated electron-hole pair density and trapping of one type of these carriers under the light-sensitive layer provide the channel required for carrier recirculation under an external bias voltage. *(v)* The latest method is the plasma wave-assisted photodetection, which is used in the modulation-doped field effect transistor (MODFET) that has a two-dimensional electron gas (2DEG) channel. The electron gas layer acts as a cavity for the excited plasma wave in the metal-semiconductor interface by light incidence, making a resonance regime. *Dyakonov and Shur* [8,

9] presented evidence that the response of this resonance regime with plasmon standing wave is a DC photovoltaic that can be measured on both sides of the source and drain of the MODFET.

In this paper, we studied the photovoltaic optical behavior of silicon p-n junction in quantum dimensions by the photovoltaic method and solved Green's functions in non-equilibrium conditions by performing first-principles calculations. Moreover, we obtained the electronic properties, dark current, and photocurrent characteristics of the studied structure. The results correspond to those previously reported by other researchers in similar cases [10].

2. Theory and Methods

In the photocurrent calculation, we consider light incidence as the first-order perturbation on the studied nanostructured electronic system. This perturbation occurs due to the interaction of the weak electromagnetic field of the incident light. The interaction of photons with electrons is described by the Hamiltonian equation (1):

$$H' = \frac{q}{m_0} \times \boldsymbol{A} \,.\, \boldsymbol{P}, \qquad (1)$$

where $\boldsymbol{A}$ and $\boldsymbol{P}$ are the potential vector and the momentum operator, respectively. Also the q is electron charge and m_0 is the mass of electron. Assuming that the incident light source is monochromatic and propagated only in the fundamental mode. Equation (2) can be used to calculate the potential vector [11]:

$$\boldsymbol{A} = \boldsymbol{e}\left(\frac{\hbar\sqrt{\tilde{\boldsymbol{\mu}}_r\tilde{\boldsymbol{\epsilon}}_r}}{2N\boldsymbol{\omega}\tilde{\boldsymbol{\epsilon}}\boldsymbol{c}}\cdot\boldsymbol{F}\right)^{1/2} \times (be^{-j\omega t} + b^{\dagger}e^{j\omega t}), \qquad (2)$$

where μ_r and ε_r are respectively relative permeability and relative permittivity coefficients, ω is the incident light frequency, $\boldsymbol{F}$ is the incident photon flux, and b and $b^{\dagger}$ are the bosonic generation and annihilation operators. Moreover, the unit vector $\boldsymbol{e}$ indicates the polarization of incident light, through which we can involve polarization effect in the simulation of optical properties.

Based on the standard *Meir-Wingreen* formulas [12], and if we include only the first order experssion in the calculation of photon flux, we obtain a equation similar to the *Fermi golden rule* for the photocurrent calculation [13]. This electric current flows due to light absorption from the left terminal (L) to the right terminal (R) and is expressed by the following formulas [14]:

$$I_\alpha = \frac{q}{\hbar}\int_{-\infty}^{\infty}\left(\sum_{\beta=L,R}\left([1-f_\alpha(E)]f_\beta(E - \hbar\boldsymbol{\omega})T^{-}_{\alpha,\beta} - f_\alpha(E)\left[1-f_\beta(E+\hbar\boldsymbol{\omega})\right]T^{+}_{\alpha,\beta}\right)\right)dE, \qquad (3)$$

$$T^{-}_{\alpha,\beta}(E) = N\,\mathrm{Tr}\left\{M^{\dagger}\tilde{A}_\alpha(E)MA_\beta(E-\hbar\boldsymbol{\omega})\right\}, \qquad (4)$$

$$T^{+}_{\alpha,\beta}(E) = N\,\mathrm{Tr}\left\{M\tilde{A}_\alpha(E)M^{\dagger}A_\beta(E+\hbar\boldsymbol{\omega})\right\}. \qquad (5)$$

In these formulas, the α index replaces letters L and R to show the corresponding relationships between the left and right terminals, respectively ($\alpha \in L, R$). Besides, the function f_α is the Fermi-Dirac distribution function of the α terminal. A_α and $\tilde{A}_\alpha$ represent the spectral function and the spectral reverse time function of the α terminal, respectively. Formula (6) describes the electron-photo coupling matrix:

$$\boldsymbol{M_{ml}} = \frac{\boldsymbol{q}}{\boldsymbol{m_0}}\left(\frac{\hbar\sqrt{\tilde{\boldsymbol{\mu}}_r\tilde{\boldsymbol{\epsilon}}_r}}{2N\boldsymbol{\omega}\tilde{\boldsymbol{\epsilon}}\boldsymbol{c}}\cdot\boldsymbol{F}\right)^{1/2} \times (\boldsymbol{e}\cdot\boldsymbol{P_{ml}}) \qquad (6)$$

By following the above steps, the overall photocurrent of the nanodevice is finally calculated from the current difference between the left and right terminals: $I_{Ph}=I_L-I_R$. In these calculations, , G and $G^{\dagger}$ functions are respectively

advanced and retarded Green's function, Γ_α is the spectral broadening function of each nanodevice terminal, and $\boldsymbol{P}$ is the momentum operator, all of which result from solving the Hamiltonian DFT-NEGF self-consistently. In this article, we implemented the above mentioned numerical analysis using the quantum ATK software package [15] developed based on python programming language [16]. In this method, we first create the atomic structure of the p-n junction as shown in Fig. 1. The definitions of positive (p) and negative (n) impurities are important challenges in atomic simulations and first-principles calculations, which are resolved in ATK software. Impurity density is considered $2\times10^{+20}$ (#/cm^3) for junction sides. In this simulator, a solution for the computerized study of adding impurity atoms is as to apply an external compensation potential, which recreates the potential effect of electrons related to the ionization of impurity atoms in a real structure. Depending on the types of impurity atoms selected for the compensation electric field based on electron or holes injected from these impurity atoms, donor or acceptor impurity is included in the calculation process. Impurity inclusion is defined in one of ATK software engineering tools in the Builder environment.

Table 1 represents the technical specifications of the designed silicon nanostructure, including the cross-section of the current (14.75 Å^2), and the direction of the current is along with the Miller index <100>.

Fig. 1 Atomic nanostraucture of studied p-n junction based on Si.

.

3. Results and discussion

Understanding the electronic structure of nanodevices is the first step in their computational study. Fig. 2 depicts the electronic density of states (DOS) spectrum of the studied device obtained from solving its DFT-NEGF Hamiltonian.

The high peak with an amplitude of 25 eV^{-1} at an $\boldsymbol{E}$ energy of about 0.60 eV refers to the highest available DOS. In negative energies, a high peak is also seen for DOS occurring with an amplitude of 23 eV^{-1} and in an $\boldsymbol{E}$ energy of about −0.55 eV. Calculating the distance between the two peaks opens a 1.15 eV bandgap energy.

Fig. 3 illustrates the quantum transmission coefficient spectrum in unbiased conditions. This coefficient is related to nanodevice electrical conductance. The presence of almost 1.15 eV bandgap energy in this spectrum confirms the semiconductor behavior of this nanostructure.

Although the transmission coefficient typically represents the probability of electron transport, and our expectation of the probability number is a value less than one, Fig. 3 shows that the quantum transmission coefficient reaches values of 3 and 2 in negative and positive energies, respectively.

Table 1 Studied Si p-n nano-device atomic configuration

DeviceConfiguration	
Central region	
Atoms	Si_{56} (56 atoms)
Selection	None
Lattice type	Unit Cell
Primitive vectors (Å)	A = [3.84, 0, 0] B = [0, 3.84, 0] C = [0, 0, 76.03]
Unit cell volume	1121 Å³
AB cross section area	14.75 Å²
Left principal layer electrode length	10.86 Å
Right principal layer electrode length	10.86 Å
Left electrode	
Atoms	Si_4 (4 atoms)
Unit cell length	5.431 Å
Right electrode	
Inequivalent to left electrode.	
Atoms	Si_4 (4 atoms)
Unit cell length	5.431 Å

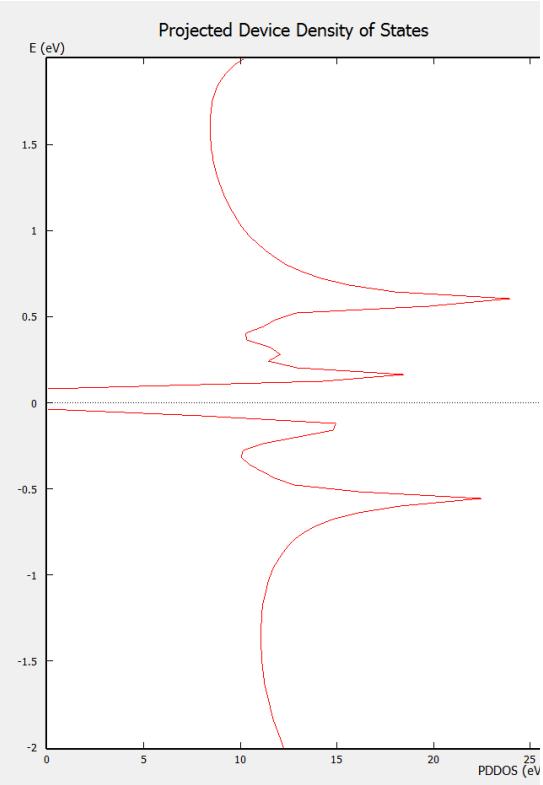

Fig. 2 Device Density of state (DDOS) that display the energy bandgap of two probe nanodevice

The physical reason for this event is the calculation of the total transmission coefficient for all quantum channels between two electrodes of the device, leading to a result beyond the one.

The diode behavior of the silicon p-n junction in its IV-curve characteristic is evident in Fig. 4.

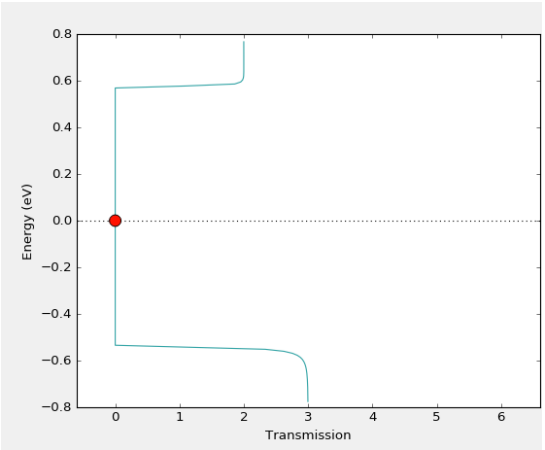

Fig. 3 Quantum transmission coefficient spectrum at zero bias condition

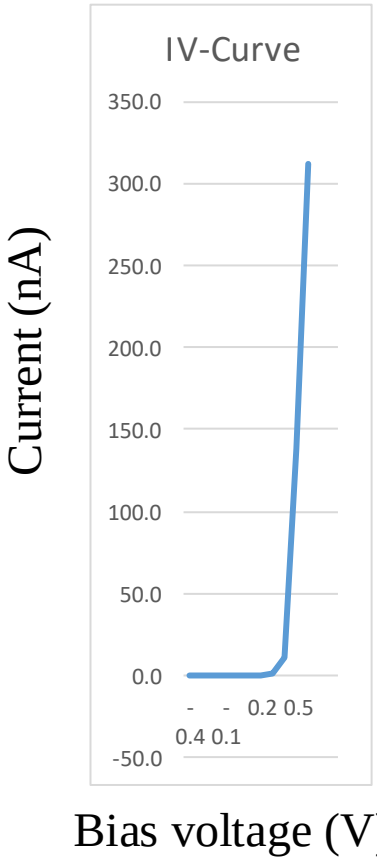

Fig. 4 IV-characteristics of Si p-n junction that represent the dark current

The near-zero current in reverse bias and the exponential increase in the current of the device for exceeding the forward bias of 0.55V indicate the diode nature of this nanostructure. In Fig. 4, the vertical axis is based on nano-amps, and the effective cross-section area for the current transfer is involved in calculating this values.

In this study, the key result is photocurrent response obtained from light incidence in a relatively broad frequency spectrum of 5 eV. Fig. 5 shows the light absorption spectrum of the present nanostructure obtained by calculating the photocurrent per incident light with different frequencies. In Fig. 5, the vertical axis is based on photocurrent density on a logarithmic scale. This spectrum indicates that the photocurrent is zero up to an energy of about 1.15 eV. This zero current in photon energies below 1.15 eV corresponds to the bandgap energy observed in the nanodevice electronic structure, which confirms the accuracy of the results obtained for the optical behavior of the device.

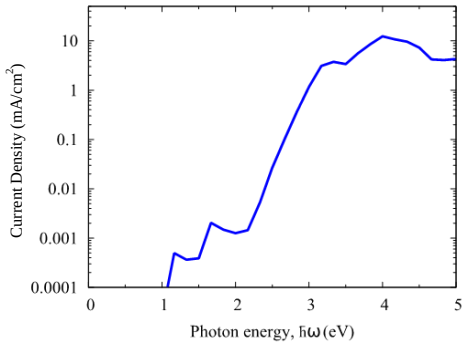

Fig. 5 Photocurrent density spectrum in log-scale representation.

4. Conclusion

The results of this study demonstrate that solving Non-Equilibrium Green's Functions is a first-principles calculations method independent of quasi-experimental coefficients to study the optical behavior of nanodevices. By relying on the first order experssion in the perturbation theory to calculate the effect of light incidence, the resulting photocurrent will be obtained from a function similar to that expressed in Fermi's golden rule. We performed our analysis solely by describing the atomic structure and determining the electrical and magnetic fields applied from the outside related to light incidence to extract photoelectrical results. Wavelengths, amplitude intensity, and polarization can be determined for incident light in the numerical analysis process. Conventional approximations in the bulk device are not accountable in the study of nanodevices, necessitating the use of *Ab initio* calculations. The results in this paper are in line with previous reliable reports of scientists who worked with an experimental or computational approach. Therefore, this developed numerical model is valid for nanostructures with quantum confinement.

5. References

[1] A. Qazi, F. Hussain, N. A. Rahim, G. Hardaker, D. Alghazzawi, K. Shaban, and K. Haruna, "Towards Sustainable Energy: A Systematic Review of Renewable Energy Sources, Technologies, and Public Opinions", *IEEE Access*, vol. 7, pp. 63837-63851, 2019.

[2] H. Melchior, M. B. Fisher, and F. R. Arams, "Photodetectors for optical communication systems", *Proceedings of the IEEE*, vol. 58, no. 10, pp. 1466-1486, 1970.

[3] I. A. Cunningham and R. Shaw, "Signal-to-noise optimization of medical imaging systems", *Journal of the Optical Society of America A*, vol. 16, no. 3, pp. 621-632, 1999.

[4] K. Ramalingam and C. Indulkar, "Chapter 3 - Solar Energy and Photovoltaic Technology," in *Distributed Generation Systems*, G. B. Gharehpetian and S. M. Mousavi Agah, Eds., ed: Butterworth-Heinemann, pp. 69-147, 2017.

[5] X. Lu, L. Sun, P. Jiang, and X. Bao, "Progress of Photodetectors Based on the Photothermoelectric Effect", *Advanced Materials*, vol. 31, no. 50, p. 1902044, 2019.

[6] P. L. Richards, "Bolometers for infrared and millimeter waves", *Journal of Applied Physics*, vol. 76, no. 1, pp. 1-24, 1994.

[7] H. Fang and W. Hu, "Photogating in Low Dimensional Photodetectors", *Advanced Science*, vol. 4, no. 12, p. 1700323, 2017.

[8] M. I. Dyakonov, "Generation and detection of Terahertz radiation by field effect transistors", *Comptes Rendus Physique*, vol. 11, no. 7, pp. 413-420, 2010.

[9] A. Satou and K. Narahara, "Numerical Characterization of Dyakonov-Shur Instability in Gated Two-Dimensional Electron Systems", *International Journal of High Speed Electronics and Systems*, vol. 25, no. 03n04, p. 1640024, 2016.

[10] [M. Palsgaard, T. Markussen, T. Gunst, M. Brandbyge, and K. Stokbro, "Efficient First-Principles Calculation of Phonon-Assisted Photocurrent in Large-Scale Solar-Cell Devices", *Physical Review Applied*, vol. 10, no. 1, p. 014026, 2018.

[11] L. E. Henrickson, "Nonequilibrium photocurrent modeling in resonant tunneling photodetectors", *Journal of Applied Physics*, vol. 91, no. 10, pp. 6273-6281, 2002.

[12] Y. Meir and N. S. Wingreen, "Landauer formula for the current through an interacting electron region", *Physical Review Letters*, vol. 68, no. 16, pp. 2512-2515, 1992.

[13] P. A. M. Dirac and N. H. D. Bohr, "The quantum theory of the emission and absorption of radiation", *Proceedings of the Royal Society of London. Series A, Containing Papers of a Mathematical and Physical Character*, vol. 114, no. 767, pp. 243-265, 1927.

[14] J. Chen, Y. Hu, and H. Guo, "First-principles analysis of photocurrent in graphene PN junctions", *Physical Review B*, vol. 85, no. 15, p. 155441, 2012.

[15] S. Smidstrup, T. Markussen, P. Vancraeyveld, J. Wellendorff, J. Schneider, T. Gunst, B. Verstichel, D. Stradi, P. A. Khomyakov, *et al.*, "QuantumATK: an integrated platform of electronic and atomic-scale modelling tools", *Journal of Physics: Condensed Matter*, vol. 32, no. 1, p. 015901, 2019.

[16] K. Hinsen, "High-Level Scientific Programming with Python," in *Computational Science — ICCS 2002: International Conference Amsterdam, The Netherlands, April 21–24, 2002 Proceedings, Part III*, P. M. A. Sloot, A. G. Hoekstra, C. J. K. Tan, and J. J. Dongarra, Eds., ed Berlin, Heidelberg: Springer Berlin Heidelberg, pp. 691-700, 2002.